Pressure-Induced Phase Transitions in $LiNH_2$

Raja S. Chellappa* and Dhanesh Chandra

Materials Science & Engineering Division, Department of Chemical & Metallurgical Engineering (MS 388), University of Nevada, Reno, Nevada 89557

Maddury Somayazulu, Stephen A. Gramsch, and Russell J. Hemley

Geophysical Laboratory, Carnegie Institution of Washington, 5251 Broad Branch Road NW, Washington, DC 20015

Received: April 25, 2007

In situ high-pressure Raman spectroscopy studies on $LiNH_2$ (lithium amide) have been performed at pressures up to 25 GPa. The pressure-induced changes in the Raman spectra of $LiNH_2$ indicates a phase transition that begins at ∼12 GPa is complete at ∼14 GPa from ambient-pressure α-$LiNH_2$ (tetragonal, $I\bar{4}$) to a high-pressure phase denoted here as β-$LiNH_2$. This phase transition is reversible upon decompression with the recovery of the α-$LiNH_2$ phase at ∼8 GPa. The N−H internal stretching modes ($\nu([NH_2]^-)$) display an increase in frequency with pressure, and a new stretching mode corresponding to high-pressure β-$LiNH_2$ phase appears at ∼12.5 GPa. Beyond ∼14 GPa, the N−H stretching modes settle into two shouldered peaks at lower frequencies. The lattice modes show rich pressure dependence exhibiting multiple splitting and become well-resolved at pressures above ∼14 GPa. This is indicative of orientational ordering $[NH_2]^-$ ions in the lattice of the high-pressure β-$LiNH_2$ phase.

I. Introduction

Alkali metals (Li, Na) and alkaline earth metals (Mg, Ca) form hydrides with complex anion species such as $[AlH_4]^-$, $[NH_2]^-$, and $[BH_4]^-$ termed as aluminohydrides (alanates), amides, and borohydrides, respectively. The large theoretical hydrogen densities (gravimetric as well as volumetric) in some of these complex hydrides[1] make them attractive for hydrogen storage for on-board vehicular applications.[2] For example, $LiBH_4$ has 18.5 wt % H_2 and ∼120 kg $H_2 \cdot m^{-3}$ that easily satisfies the USDOE 2010 goal for FreedomCAR which is 9 wt % H_2 and ∼45 kg $H_2 \cdot m^{-3}$. These hydrides are characterized by strong metal−hydrogen bonding (Al−H, N−H, and B−H) in the anion group;[3] in order to facilitate hydrogen desorption, a weakening of the metal−hydrogen bond in the anion complexes is necessary. Furthermore, the desorbed hydride (partially or fully) should be metastable enough to revert to the original hydride phase upon hydrogenation. One technique that has proved useful for such pre-processing and catalyst addition (usually Ti-based[4]) is ball-milling.[5−7] *In situ* powder diffraction and vibrational spectroscopy have revealed some underlying catalyst mechanisms of catalyst action, but there are still unresolved issues.[8−10] Following the pioneering work by Chen et al.[11] on the Li−N−H system ($Li_3N \leftrightarrow Li_2NH \leftrightarrow LiNH_2$) for hydrogen storage, numerous reports[12,13] have appeared on the amide/imide system. Recent efforts involve the ball-milling of $LiNH_2$ with other complex hydrides ($LiBH_4$, $LiAlH_4$) to obtain a reversible hydrogen storage material.[14]

The formation of metastable high-pressure phases and pressure-induced instabilities during ball-milling (materials being crushed experience pressures up to 6 GPa[15−17]) is a distinct possibility.[18,19] A deeper understanding of the pressure-induced transformations in these complex hydrides can provide insights into effects of pressure on the metal−hydrogen bonding and its implications for hydrogen desorption/absorption. In our previous study[20] on $LiAlH_4$, a high-pressure phase transition (α-$LiAlH_4$ transforms to β-$LiAlH_4$ at ∼3 GPa) was confirmed. In addition, it was also suggested that pressure-induced weakening of an Al−H bond and emergence of disorder can be related to the facilitation of hydrogen desorption from complex hydrides.[21] Other high-pressure studies on $LiAlH_4$,[22−24] $NaBH_4$,[25,26] and $LiBH_4$[27] have reported on the extent of densification and order/disorder effects in the high-pressure phases.

Here, we present a high-pressure Raman spectroscopy study of $LiNH_2$ up to 25 GPa in a diamond anvil cell (DAC) to identify pressure-induced phase transitions and elucidate the vibrational behavior of the $[NH_2]^-$ anion complex at higher pressures.

II. Experimental

Reagent grade $LiNH_2$ powder of 95% purity was purchased from Sigma Aldrich Inc. and was used without further purification. The high-pressure Raman spectroscopy experiments performed in this work were carried out at the Geophysical Laboratory (GL) at the Carnegie Institution of Washington (CIW), Washington, DC. The DAC used for the Raman spectroscopy[28] studies had diamonds with 300 μm culets, and samples were loaded in rhenium gaskets with holes of 100−125 μm. The sample loadings were performed in a glove box (Ar atmosphere) without any pressure-transmitting medium to avoid any possible reactions with commonly used media such as 4:1 methanol/ethanol. The ruby (Cr^{+3}-doped α-Al_2O_3) fluorescence method (R_1 line at 694.2 nm under ambient conditions) was used to determine the pressure inside the DAC.[29] Two or three ruby chips were included with the sample for

* Corresponding author. Address: Geophysical Laboratory, Carnegie Institution of Washington, 5251 Broad Branch Road, NW, Washington, DC 20015; Ph: (202) 478-8926; Fax: (202) 478-8901; E-mail: rchellappa@ciw.edu.

10.1021/jp073206w CCC: $37.00
Published on Web 08/21/2007

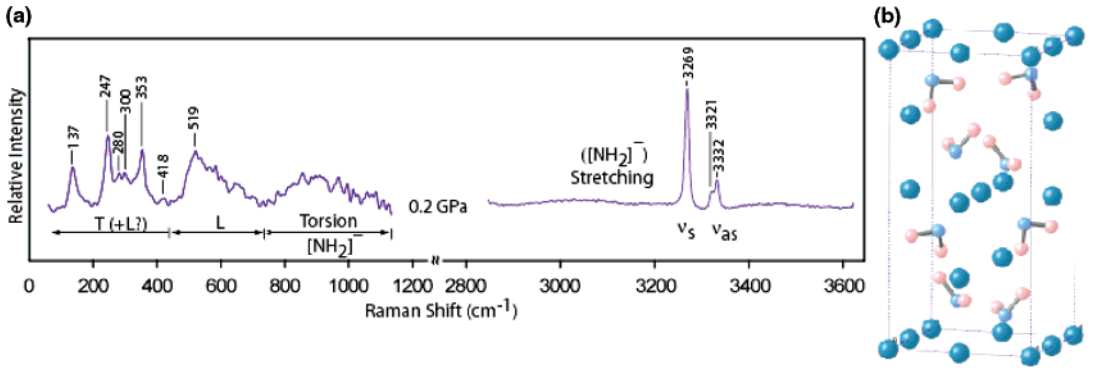

Figure 1. (a) Raman mode assignments of the as-loaded (~0.2 GPa) $LiNH_2$ sample. The lattice translational (T) and librational (L) are prominent and as discussed in the text; the translational and librational motions may be coupled. The internal torsional modes wagging (ω), rocking (ρ), and twisting (τ) appear as unresolved broad peaks (beyond 800 cm^{-1}); however, not much activity was observed in this region with increasing pressure, so the internal torsional assignment is tentative. The N−H stretching modes (ν_s and ν_{as}) are well-resolved. (b) The crystal structure of $LiNH_2$ ($I\bar{4}$) is shown (Li: large blue spheres, N: small light-blue spheres, H: small pink spheres, Color Online).

monitoring the presence of pressure gradients. For the pressures measured in this study, the R_1 and R_2 lines remained well-resolved with a separation of ~29 cm^{-1}, suggesting reasonably quasi-hydrostatic conditions within the sample volume. The DAC was assembled and sealed with minimal initial pressure (initial pressure varied from ~0.2 to 1.3 GPa). Raman measurements were performed using the 488 nm line of an Ar^+ laser (Coherent Innova 90). The imaging spectrograph (ISA HR460, 300 and 1800-grooves/mm grating) equipped with a liquid-nitrogen-cooled charge-coupled device (CCD) detector with a 460 mm focal length *f*/5.3 was used, providing a resolution of 0.5 cm^{-1}. The Raman scattering wavelength was calibrated using Ne lines providing an accuracy of 1 cm^{-1}. We note here that the Raman active modes near the first-order diamond peak at 1331 cm^{-1} cannot be studied due to the very high intensity of this peak. Therefore, first an overall spectrum with 300 grooves/mm grating was collected, and it was decided that the spectra in the ranges of 100−1200 and 2800−3600 cm^{-1} would be monitored with the higher-resolution 1800 grooves/mm grating. The δ(HNH) deformation mode is expected around 1500 cm^{-1} for $LiNH_2$ but was not monitored in this study.

III. Results and Discussion

III.A. Vibrational Mode Assignment of Pure $LiNH_2$. In order to interpret the pressure-induced changes in Raman spectra, it is desirable to have a full assignment of Raman modes in $LiNH_2$. There are only two detailed vibrational spectroscopic studies on $LiNH_2$—an IR study in 1965 by Novak et al.[30] from 300 to 3700 cm^{-1} and a Raman study in 1995 by Bohger et al.[31] from 1100 to 3400 cm^{-1}. The crystal structure of ambient-pressure α-$LiNH_2$ is tetragonal ($I\bar{4}$, $Z = 8$, $a = b = 5.03442$ Å, $c = 10.25558$ Å).[32] The total number of vibrations per Bravais primitive unit cell is 48 that can be classified as $10A + 12B + 13E$ using simple factor group analysis (FGA).[33] Further classification reveals $10A + 11B + 12E$ optical modes which consists of 21 translational ($4A + 5B + 6E$), 12 librational ($3A + 3B + 3E$), and 12 internal ($3A + 3B + 3E$) modes. The *B* and *E* modes are both IR-and Raman-active while *A* modes are Raman-active only. In this study, we were able to obtain high-resolution spectra down to 100 cm^{-1}, and we were able to clearly identify Raman features due to external (lattice) and internal vibrations. The raw Raman spectral data for all pressure increments (three runs) were smoothed using a FFT smoothing routine and then the background was subtracted. The peaks were extracted from the smoothed data, and a peak-fitting routine was used to identify shouldered peaks. The Raman spectrum of the as-loaded sample (~0.2 GPa) is shown along with the crystal structure in Figure 1.

III.A.1. External Modes. Complex librational motions of $[NH_2]^-$ ion and vibronic coupling have been reported in $NaNH_2$,[34] KNH_2,[35] and others.[36,37] Novak et al.[30] reported "lattice vibrations" at 450 and 571 cm^{-1} for $LiNH_2$ and 450 and 560 cm^{-1} for $LiND_2$ in their IR study. From the isotopic substitution rule, it follows that the modes at 450 and 571 cm^{-1} can be assigned to translational and librational motions, respectively. Cunningham and Maroni[34] also reported Raman modes due to $[NH_2]^-$ librations at 349, 468, and 522 cm^{-1} in α-$LiNH_2$. Neutron scattering studies of $NaNH_2$[38] suggest weak $[NH_2]^-$ torsion at ~400 cm^{-1}, a strong wagging peak at 550 cm^{-1}, and a broad peak of medium intensity due to rocking at 1000 cm^{-1}. A high-frequency translatory lattice mode (345 cm^{-1}) has also been reported in $Ca(NH_2)_2$.[39] In light of these studies, the assignment of the lattice modes in this study (for the lowest measured pressure ~0.2 GPa) are (1) *translational modes* at 137, 247, 280, 300, 353, and 418 cm^{-1} and (2) *librational mode* at ~519 cm^{-1} (broad peak). The broad peak centered around 900 cm^{-1} is tentatively assigned to torsion, and it is noted that this mode remained unresolved and did not exhibit much activity with increasing pressure.

III.A.2. Internal Modes. There are three fundamental internal vibrations associated with the $[NH_2]^-$ anion: in-plane bending modes $\nu_2(A_1$, H−N−H deformation), in-plane $\nu_1(A_1$, N−H symmetric stretching), and in-plane $\nu_3(B_1$, N−H asymmetric stretching). The observed values from the as-loaded sample in this study are the following: symmetric stretching frequency $\nu_s = 3269$ cm^{-1}, a shouldered asymmetric frequency $\nu_{as} = 3332$ cm^{-1}. These values are close to the free ion frequencies, suggesting the lack of any hydrogen bonding[40] in the crystal. An absence of hydrogen bonding has also been observed in $NaNH_2$.[38] As expected, the Raman spectrum of the as-loaded sample in Figure 1 shows a more intense symmetric stretching vibration than the asymmetric (the intensities are comparable in IR spectra). It is noted that the effect of the lowered site symmetry of $[NH_2]^-$ does not result in factor group splitting in the stretching modes as observed in $NaNH_2$[38] and $Ca(NH_2)_2$[39] as well. In this study, we did not record the spectra in the 1200−2800 cm^{-1} region (intense first-order diamond peak is at 1331 cm^{-1}). Thus, the bending modes (in the vicinity of 1500 cm^{-1}) were not observed.

III.B. Raman Frequencies as a Function of Pressure. The pressure-induced changes in the Raman frequencies of both external and internal modes of $LiNH_2$ exhibit complex behavior.

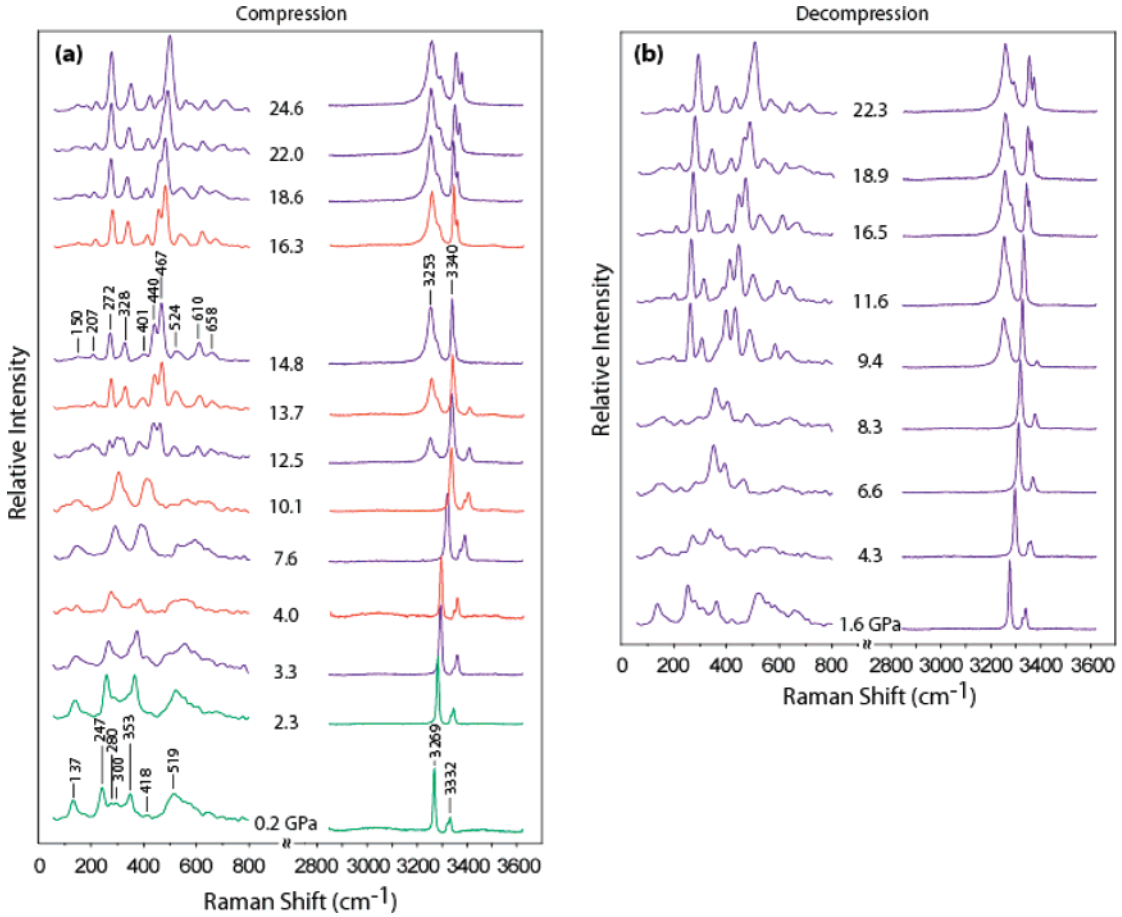

Figure 2. Raman spectra as a function of pressure are shown for (a) compression, and (b) decompression. During compression, the phase transition from α-$LiNH_2$ (tetragonal) to β-$LiNH_2$ (unknown structure) begins at ~12 GPa and is complete at ~14 GPa. During decompression, the reverse phase transition occurs between 9.4 and 8.3 GPa. The three runs are color-coded; Run 1 (green), Run 2 (blue), and Run 3 (red).

A compilation of the Raman spectra as a function of pressure during compression and decompression is given in Figure 2. The bulk of the compilation (color-coded) comes from Run 2, while some selected pressure increments from Runs 1 and 3 are also given. The spectra recorded during decompression are shown only for Run 2. A visual inspection of the Raman spectra as a function of pressure reveals the following major features:

- The lattice translational modes (possibly coupled with librations) up to 450 cm^{-1} (which appear overlapped at the lowest pressure ~0.2 GPa) split into well-resolved sharp peaks above ~14 GPa.
- The librational modes (500−800 cm^{-1}) which were overlapped in a broad peak at 519 cm^{-1} (~0.2 GPa) split into three shouldered peaks of medium intensity beyond the phase transition pressure (~14 GPa).
- During compression, the N−H stretching modes display an increase in frequency and a new mode appears at ~12 GPa that is a clear evidence for a phase transition. The transformation is complete at ~14 GPa as the stretching modes settle into two peaks at lower frequencies.
- A large hysteresis was observed to accompany the phase transition upon decompression; the β-$LiNH_2$ transformed back to α-$LiNH_2$ between 9.4 and 8.3 GPa. The midpoint between compression and decompression onset is 10.5 GPa.

III.B.1. External Modes. The pressure-induced changes in the lattice translational and librational modes can be related to symmetry changes, orientational dynamics, and ordering (or lack thereof). In $LiNH_2$, with increasing pressure, it can be seen that the mode at 137 cm^{-1} broadens slightly and shifts to higher frequency with a small slope ($d\nu/dP = 1.4$ cm^{-1}/GPa) as shown in Figure 3. It can also be observed that shoulders are developing for this mode that split into 3 modes of very low intensity beyond the phase transformation pressure. In fact, the threefold splitting can be seen clearly only beyond 17 GPa. The dominant translational modes at the lowest-pressure measurement are at 247 cm^{-1} ($d\nu/dP = 4.3$ cm^{-1}/GPa) and 353 cm^{-1} ($d\nu/dP = 6.6$ cm^{-1}/GPa). These modes continue to be dominant, while exhibiting some broadening as well as merging with the weak modes at 280 and 300 cm^{-1}. This trend continues up to ~10 GPa, beyond which we see only two modes. From ~10 to ~13 GPa, there is increased activity accompanied by multiple splitting of these modes; at ~14.8 GPa, we see five distinct peaks at 272, 328, 401, 440, and 467 cm^{-1}. The broad librational mode at 519 cm^{-1} at ~0.2 GPa also splits into three modes of medium intensity beyond ~14 GPa. The three librational modes in the high-pressure β-$LiNH_2$ phase are assigned to wagging and twisting motions of the $[NH_2]^-$ ion. The broad mode ~900 cm^{-1} shown in the ambient-pressure spectrum from 800 to 1000 cm^{-1} did not exhibit any noticeable changes with pressure, and hence it has been excluded from Figure 2. The observed mode splitting in a plot of Raman shift versus P (Figure 3) provide an indication of phase transition. The vibrational spectra recorded during decompression show a trend similar to that of compression, with a large hysteresis in the onset pressure of the transformation (~9.4 GPa during decompression and ~12 GPa during compression). The changes in volume as a function of pressure are not available at this time, and therefore the mode Grüneisen parameters were not determined.

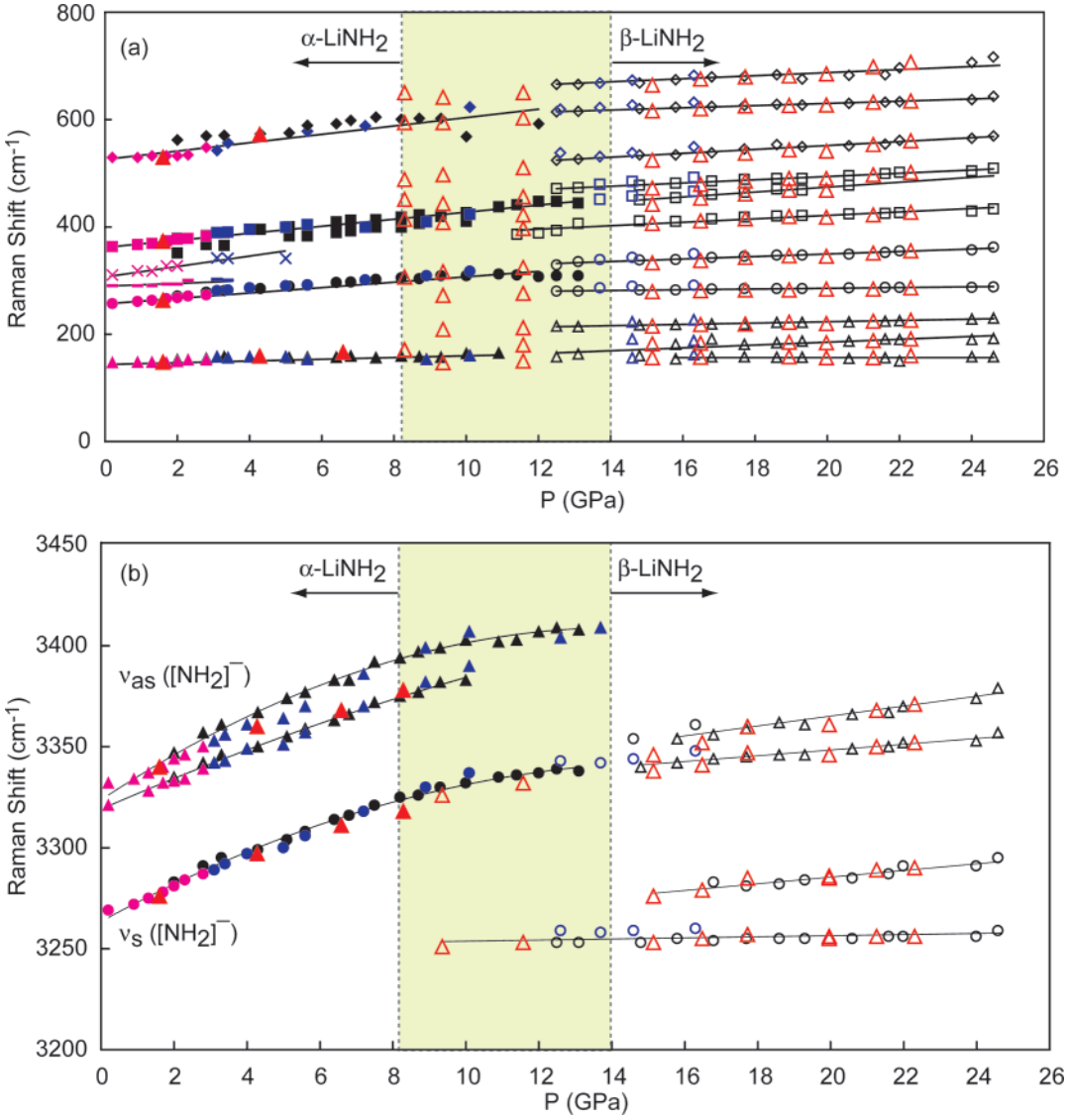

Figure 3. Raman shift of (a) lattice modes (translational and librational) and (b) N−H stretching modes as a function of pressure (the bulk of the data points are compression except red triangles which are from decompression). The increased mode splitting of the lattice modes as well as the discontinuous shifts in N−H stretching modes are a clear indication of phase transition between ~12 GPa and ~14 GPa during compression and between ~8 GPa and ~9 GPa during decompression.

III.B.2. Internal Modes. It can be seen from Figure 2 that both symmetric and asymmetric N−H stretching modes shift to higher frequencies with increasing pressure indicating a lack of formation of hydrogen bonding (at least until the phase transition). At ~12.5 GPa, an additional mode prominently appears at 3259 cm^{-1}, suggesting the beginning of a phase transition. This new mode is broad with a weak shoulder increasing in intensity with pressure; it is suggested that this new mode at lower frequency is due to the symmetric stretching in β-$LiNH_2$. However, the phase transition is not complete as the N−H stretching modes from the α-$LiNH_2$ phase continue to persist up to ~14 GPa. The phase transition to β-$LiNH_2$ is complete beyond ~14 GPa with the symmetric and asymmetric stretching modes at 3253 and 3340 cm^{-1} (~14.8 GPa), respectively. The Raman shift of the symmetric stretching mode as a function of pressure is parabolic as seen from Figure 3b. In β-$LiNH_2$, with increasing pressure the shoulders associated with the N−H stretching modes get stronger; this suggests the possibility of additional high-pressure transitions.

III.B.3. Discussion. To the best of our knowledge, this is the first high-pressure study on any alkali amide. The pressure-induced changes in Raman spectra suggest that $LiNH_2$ undergoes an ordering effect similar to $NaBH_4$.[25,26] This is unlike the high-pressure phase of $LiAlH_4$[20] where considerable peak broadening and merging of the lattice modes indicate at least partial disorder. In addition to the diffuse appearance of lattice modes (<500 cm^{-1}), the presence of broad overlapped peaks of librations (lowered energy barrier) of $[NH_2]^-$ anions (500−1000 cm^{-1}) indicate the presence of orientational disorder in the ambient-pressure α-$LiNH_2$ phase. In contrast, the high-pressure β-$LiNH_2$ phase exhibits multiple splitting, sharpening (well-resolved), and increased intensity of lattice modes that are typical of an ordering phenomenon. The crystal structure of β-$LiNH_2$ is not known but the increased number of lattice modes is an indication of lowering of symmetry from the α-$LiNH_2$ structure or a larger unit cell. It is still not evident if the N−H stretching modes at much lower frequencies in the high-pressure β-$LiNH_2$ phase are associated with the formation of hydrogen bonds or are due to structural consideration. In general, such lowering of frequencies can be associated with weakening of the N−H bonds as well as increased anharmonicities. It is pointed out that the temperature-induced orientational order−disorder phenomenon

is fairly common in alkali and alkaline-earth amides. For example, KNH_2 undergoes a transition from an ordered, low-temperature monoclinic phase ($T \leq 326$ K) to high-temperature, orientationally disordered tetragonal (326 K $\leq T \leq$ 348 K) and cubic ($T \geq 348$ K) phases. The effect on ordering of pressure is opposite to that of temperature. In general, it will be useful to determine if there is any correlation between ordering or disordering (due to pressure or temperature) and to identify any beneficial effects on hydrogen desorption/absorption characteristics of complex hydrides.

IV. Conclusions

High-pressure *in situ* Raman spectroscopy of $LiNH_2$ reveal a structural phase transition from ambient-pressure α-$LiNH_2$ (tetragonal) to a phase called here as β-$LiNH_2$, at 298 K. A large hysteresis is observed with the onset of this phase transition ~12 GPa (complete by ~14 GPa) and ~9.4 GPa (complete by 8.3 GPa), on decompression. In the low-pressure α-$LiNH_2$ phase, the presence of broad overlapped peaks due to librations of $[NH_2]^-$ ion, low-intensity lattice modes, and apparent lack of crystal field effects on the vibrational modes is attributed to the presence of orientational disorder. The high-pressure β-$LiNH_2$ phase is characterized by multiple mode splitting (external and internal), and the sharpened lattice modes suggest an orientational ordering of $[NH_2]^-$ ions in the lattice. High-pressure diffraction studies will be useful to identify the crystal structure of β-$LiNH_2$ and to confirm the existence of pressure-induced ordering.

Acknowledgment. We thank the financial support of US Department of Energy (USDOE) grants DE-FG-02-06ER46280 and Carnegie/DOE Alliance Center (CDAC) grant DE-FC-03-03NA00144.

References and Notes

(1) Schlapbach, L.; Züttel, A. *Nature* **2001**, *414*, 353.
(2) Chandra, D.; Reilly, J.; Chellappa, R. *J. Metals* **2006**, *58*, 26.
(3) Yoshino, M.; Komiya, K.; Takahashi, Y.; Shinzato, Y.; Yukawa, H.; Morinaga, M. *J. Alloys Compd.* **2005**, *185*, 404−406.
(4) Bogdanovic, B.; Schwickardi, M. *J. Alloys Compd.* **1997**, *1*, 253−254.
(5) Grochala, W.; Edwards, P. P. *Chem. Rev.* **2004**, *104*, 1283.
(6) Jensen, C. M.; et al. *Int. J. Hydrogen Energy* **1999**, *24*, 41.
(7) Zaluska, L.; Zaluski; Ström-Olsen, J. O. *J. Alloys Compd.* **2000**, *298*, 125.
(8) Balema, V. P.; Balema, L. *Phys. Chem. Chem. Phys*. **2005**, *7*, 1310.
(9) Gross, K. J.; Majzoub, E. H.; Spangler, S. W. *J. Alloys Compd.* **2003**, *423*, 356−357.
(10) Majzoub, E. H.; McCarty, K. F.; Ozolins, V. *Phys. Rev. B* **2005**, *71*, 024118.
(11) Chen, P.; et al. *Nature* **2002**, *420*, 302.
(12) Janot, R. *Ann. Chim. Sci. Mater*. **2005**, *30*, 505.
(13) Ichikawa, T.; Leng, H. Y.; Isobe, S.; Hanada, N.; Fujii, H. *J. Power Sources* **2006**, *159*, 126.
(14) Lu, J.; Fang, Z. Z.; Sohn, H. Y. *J. Phys. Chem. B* **2006**, *110*, 14236; Janot, R.; Eymery, J.-B.; Tarascon, J.-M. *J. Phys. Chem. C* **2007**, *111*, 2335.
(15) Suryanarayana, C. *Prog. Mater. Sci*. **2001**, *1*, 46.
(16) Maurice, D. R.; Courtney, T. H. *Metall. Trans. A* **1990**, *21*, 289.
(17) Weeber, A. W.; Wester, A. J. H.; Haag, W. J.; Bakker, H. *Physica B* **1987**, *145*, 349.
(18) Balema, V. P.; Dennis, K. W.; Pecharksy, V. K. *Chem. Commun.* **2000**, *17*, 1665.
(19) Balema, V. P.; Balema, L. *Phys. Chem. Chem. Phys*. **2005**, *7*, 1310.
(20) Chellappa, R. S.; Chandra, D.; Gramsch, S. A.; Hemley, R. J.; Lin, J.-F.; Song, Y. *J. Phys. Chem. B* **2006**, *106*, 11088.
(21) Andreasen, T.; Vegge, A. S.; Pedersen, *J. Solid State Chem*. **2005**, *178*, 3664.
(22) Vajeeston, P.; Ravindran, P.; Vidya, R.; Fjellvag, H.; Kjekshus, A. *Phys. Rev. B* **2003**, *68*, 212101.
(23) Talyzin, A. V.; Sundqvist, B. *Phys. Rev. B* **2004**, *70*, 180101.
(24) Pitt, M. P.; Blanchard, D.; Hauback, B. C.; Fjellvåg, H.; Marshall, W. G. *Phys. Rev. B* **2005**, *72*, 214113.
(25) Araújo, C. M.; Ahuja, R.; Talyzin, A. V.; Sundqvist, B. *Phys. Rev. B* **2005**, *72*, 054125.
(26) Sundqvist, B.; Andersson, O. *Phys. Rev. B* **2006**, *73*, 092102.
(27) Talyzin, A. V.; Andersson, O.; Sundqvist, B.; Kurnosov, A.; Dubrovinsky, L. *J. Solid State Chem.* **2007**, *180*, 510.
(28) Raman, C. V.; Krishnan, K. S. *Nature* **1928**, *121*, 711.
(29) Gillet, P.; Hemley, R. J.; McMillan, P. F. *Rev. Mineral.*; **1998**, *37*, 525−581.
(30) Novak; Josik, P.; Bouclier, P. *Compt. Rend. Acad. Sci.* **1965**, *261* (2(Groupe 8)), 455.
(31) Bohger, J.-P. O.; Essmann, R. R.; Jacobs, H. *J. Mol. Struct.* **1995**, *348*, 325.
(32) Yang, J. B.; Zhou, X. D.; Cai, Q.; James, W. J.; Yelon, W. B. *Appl. Phys. Lett.* **2006**, *88*, 041914.
(33) Rousseau, D. L.; Bauman, R. P.; Porto, S. P. S. *J. Raman Spectrosc*. **1981**, *10*, 253.
(34) Cunningham, P. T.; Maroni, V. A. *J. Chem. Phys.* **1972**, 57, 1415.
(35) Müller, M.; Senker, J.; Asmussen, B.; Press, W.; Jacobs, H.; Kockelmann, W.; Mayer, H. M.; Ibberson, R. M. *J. Chem. Phys.* **1997**, *107*, 2363; *J. Chem. Phys.* **1998**, *109*, 3559.
(36) Senker, J.; Jacobs, H.; Müller, M.; Press, W.; Müller, P.; Mayer, H. M.; Ibberson, R. M. *J. Phys. Chem. B* **1998**, *102*, 931.
(37) Senker, J.; Jacobs, H.; Müller, M.; Press, W.; Neue, G. *J. Phys. Chem. B* **1999**, *103*, 4497.
(38) Day, D. H.; Sinclair, R. N. *J. Chem. Phys.* **1971**, *55*, 2807.
(39) Bouclier, P.; Portier, J.; Turrell, G. *J. Mol. Struct.* **1968**, *4*, 1.
(40) Lutz, H. D. *J. Mol. Struct*. **2003**, *646*, 227.